THE JOURNAL OF PHYSICAL CHEMISTRY B
A JOURNAL OF THE AMERICAN CHEMICAL SOCIETY

pubs.acs.org/JPCB

Article

Heavy-Atom Tunneling in the Covalent/Dative Bond Complexation of Cyclo[18]carbon−Piperidine

Ashim Nandi* and Jan M. L. Martin*

Cite This: *J. Phys. Chem. B* 2022, 126, 1799−1804

Read Online

ACCESS | Metrics & More | Article Recommendations | Supporting Information

ABSTRACT: Recent quantum chemical computations demonstrated the electron-acceptance behavior of this highly reactive cyclo[18]carbon (C_{18}) ring with piperidine (pip). The C_{18}−pip complexation exhibited a double-well potential along the N−C reaction coordinate, forming a van der Waals (vdW) adduct and a more stable, strong covalent/dative bond (DB) complex by overcoming a low activation barrier. By means of direct dynamical computations using canonical variational transition state theory (CVT), including the small-curvature tunneling (SCT), we show the conspicuous role of heavy atom quantum mechanical tunneling (QMT) in the transformation of vdW to DB complex in the solvent phase near absolute zero. Below 50 K, the reaction is entirely driven by QMT, while at 30 K, the QMT rate is too rapid ($k_T \sim 0.02\ s^{-1}$), corresponding to a half-life time of 38 s, indicating that the vdW adduct will have a fleeting existence. We also explored the QMT rates of other cyclo[n]carbon−pip systems. This study sheds light on the decisive role of QMT in the covalent/DB formation of the C_{18}−pip complex at cryogenic temperatures.

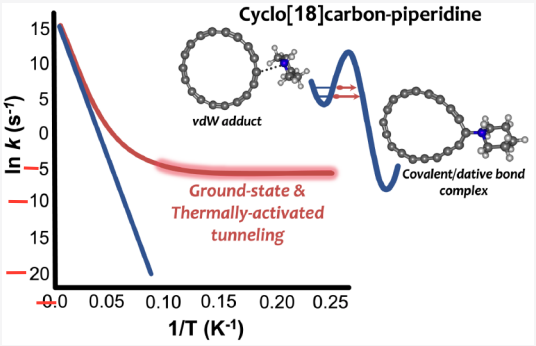

INTRODUCTION

Because of its unique electronic and structural features, the newly synthesized sp-hybridized cyclo[18]carbon (C_{18}) ring has sparked widespread attention to both theoreticians and experimentalists since its first experimental observation in condensed media in 2019.[1] The successful *in situ* generation and characterization of this decades-old elusive C_{18} ring via atom manipulation by an atomic force microscope (AFM) tip was a landmark study because of the potential to be an alternate candidate for pure carbon allotropes.[2−4] Following this experimental feat, several theoretical studies have explored the geometrical structure and stability of the C_{18} ring in the gas phase,[5−10] and more importantly, a series of interesting properties have been highlighted, such as the electronic and transport properties,[8,11−15] double aromatic character,[16−18] dynamics behavior,[6] and so on—most of these studies revolved around the noncovalent interaction of C_{18} with other elements or molecular entities.

In a recent combined experimental and theoretical study by Hobza's group,[19] it was shown that an sp^2-hybridized carbon allotrope, namely C_{60}, forms a strong N → C dative bond with piperidine (pip), thereby explaining the long-standing question on the enhanced stability of C_{60} with pip compared to other organic or inorganic solvents.[20,21] In contrast, planar carbon allotropes (graphene and nanotubes) form only noncovalent interactions with pip.[22] Stimulated by these works, the same group theoretically studied the electron-acceptance potential of C_{18} with pip in the gas phase and continuum solvent (using the pip dielectric constant).[23] According to their DFT computations at the ωB97XD/def2-TZVPP level, the C_{18}−pip complex was predicted to exhibit double-well potentials along the N−C reaction coordinate, first forming a weak van der Waals (vdW) adduct with a long N−C bond (3.006 Å), followed by a thermodynamically stable strong dative bond (DB) complex with a short N−C bond (1.501 Å). The vdW → DB transformation was low (activation barrier $\Delta E^{\ddagger}$ = 3.2 kcal mol^{-1}) and highly exergonic (reaction energy ΔE_r = −12.6 kcal mol^{-1}) in the gas phase, taking the vdW complex as a reference. Extra stabilization of the C_{18}−pip complex was predicted upon moving to the solvent phase. NBO analysis and molecular dynamics simulation further revealed the stability of the DB complex at room temperature.

Additionally, they have investigated the stability of other hypothetical cyclo[n]carbon systems with pip. Noteworthy, prior to the vdW complexation, their computations also predicted a stable hydrogen-bonded complex where hydrogen from N−H forms a bond with C_{18} and its relative energy lies 1 kcal mol^{-1} above the vdW complex in the gas phase. Encouraged by the low activation barrier for the vdW → DB process in C_{18}−pip and more importantly by the high

Received: January 11, 2022
Revised: February 5, 2022
Published: February 18, 2022

exergonicity of the reaction, which may yield a narrow effective barrier width in accord with Hammond's postulate,[24] we wondered if this reaction can be driven by heavy-atom quantum mechanical tunneling (QMT) even close to absolute zero.

Reactions involving QMT by heavy atoms (mostly second-row elements of the periodic table)[25−28] are relatively rare compared to light hydrogen tunneling-based reactions; however, recent years have witnessed the slow emergence of heavy-atom QMT, especially in organic chemistry.[25,28,29] This nonclassical QMT phenomenon is a well-known effect that significantly accelerates reaction rates by passing through the potential barrier instead of crossing over it.[30,31] The extent to which QMT occurs in a chemical reaction can be approximated according to $P \sim e^{-w\sqrt{\Delta E^{\ddagger} m}/\hbar}$, where P is the tunneling probability, w is the barrier width, $\Delta E^{\ddagger}$ is the activation energy, and m is the mass of the moving parts of the molecule.[26,27] Clearly, among these three factors that determine the tunneling probability, the barrier width has the most decisive influence on the tunneling probability. Indeed, several experimental and/or computational studies have demonstrated that the characteristic features of reactions driven by heavy-atom QMT are their low and narrow barriers.[25,28,29] The few documented cases include pericyclic[32] and degenerate rearrangement reactions involving carbon,[33−35] fluoride,[36,37] and boron[38] tunneling. Carbon and nitrogen tunneling in highly exergonic reactions in reactive intermediate species, such as carbene or nitrene, has also been reported.[39−41] Recently, boron atom tunneling has been predicted in the highly exergonic reaction involving the N−B bond-stretch isomerization of nitrile−boron halides, whereby the metastable vdW adduct isomerizes to a global minimum covalent/dative bond complex.[42]

In this work, through direct dynamics computations, we show the dominant role of heavy-atom tunneling in the transformation of vdW → DB in the C_{18}−pip complex near absolute zero in the solvent phase. We also extend our tunneling results to other cyclo[n]carbon−pip (n = 14, 16, 18, 20, and 22). This study may elucidate the possibility of leveraging the role of QMT in the dative/covalent functionalization of the C_{18}−pip complex.

COMPUTATIONAL METHODS

All of the DFT electronic structure calculations were performed at the M06-2X[43]/def2-TZVP level with the Gaussian 16 program suite.[44] This level of theory was chosen since it correctly reproduces the observed polyynic structure of cyclo[18]carbon.[6,8] In addition, it was shown to closely match the minimum potential energy surface (PES) of C_{18} against DLPNO-CCSD(T)-F12 computations,[6] which is crucial for our accurate direct dynamical studies. The SCF convergence criteria were set by using the keyword "opt = tight", which sets the maximum and root-mean-square (RMS) forces to 1.5×10^{-5} and 1.0×10^{-5} hartree/bohr and the maximum and RMS displacements to 6.0×10^{-5} and 4.0×10^{-5} bohr. The "ultrafine" grid, which is a pruned direct product of a 99-point Euler−MacLaurin radial grid combined with a 590-point Lebedev angular grid,[45] was employed for all DFT calculations. Intrinsic reaction coordinate (IRC) calculations were conducted to confirm that the transition state is smoothly connected to the reactant and product side.

The semiclassical rate constants were computed by using canonical variational transition state theory (CVT),[46] while the tunneling rates were accounted for by using the highly demanding multidimensional small curvature tunneling (SCT) method.[47,48] We refer to the semiclassical CVT and the tunneling-corrected SCT rates as k_{SC} and k_T. Polyrate17[49] was used to compute all the rate constants, with Gaussrate17[50] serving as the interface between Polyrate and Gaussian. The Page−McIver algorithm[51] with a gradient and a Hessian step size of 0.002 and 0.018 bohr (the smallest standard recommended step size for Polyrate calculation)[49] was employed to map the reaction energy path for all the studied reactions. Quantized reactant state tunneling (QRST)[52] calculations were used to obtain accurate rate constants at the subcryogenic temperatures. Geometry optimization and the rate constant calculations in the solvent phase were taken into account by using the integral equation-formalism polarizable continuum model (IEFPCM)[53] with a dielectric constant of 5.9 (a value for piperidine solvent). For the sake of reproducibility of our QMT computations, and due to the number of keywords involved that can slightly affect the rates, a sample Polyrate input file is provided in the Supporting Information.

All of the energetics, namely binding (BE), threshold barrier ($\Delta E^{\ddagger}$), and the reaction (ΔE_r) energies, reported throughout this work are in the continuum piperidine solvent phase unless otherwise mentioned and include the zero-point energy corrections.

RESULTS AND DISCUSSION

As a starting point, we considered the double-well potential of the donor−acceptor C_{18}−pip complex reported by Hobza and co-workers described above. Our gas-phase computations at the M06-2X/def2-TZVP level yield an N−C long-bond and short-bond complex with a bond distance of 3.016 and 1.496 Å, and the corresponding binding energies (BE, without zero-point energy correction) are −3.0 and −12.0 kcal mol^{-1}, characteristics of a van der Waals (vdW) complex and a covalent/dative bond (DB) for the former and latter. These two distinct minima are separated by a low threshold barrier ($\Delta E^{\ddagger}$) of 3.5 kcal mol^{-1} from the vdW complex, with a corresponding reaction energy (ΔE_r) of −9.1 kcal mol^{-1}, in close agreement with the reported DFT and DLPNO−CCSD(T) computations,[23] indicating the suitability of our selected level of theory. As mentioned above, inclusion of implicit solvent was shown to stabilize the C_{18}−pip, and indeed, upon transitioning our computations to the solvent phase, the threshold barrier (2.2 kcal mol^{-1}) is significantly lowered and the reaction energy (−17.7 kcal mol^{-1}) becomes more exergonic, indicating the extra stability of the transition state and the DB complex exerted by the solvent as compared to the vdW adduct. Figure 1 depicts the N−C bond distances and the energetics of the double-well potential profile of C_{18}−pip in the pip solvent.

Considering the low threshold barrier and high exergonicity of the above reaction, we embarked on investigating accurate QMT rates of this chemical transformation. Our computed tunneling rate constants reveal that the reaction is wholly dominated by ground-state QMT near absolute zero. In fact, at 4 K, the calculation shows that the classical over-the-barrier process is impossible, with a k_{SC} of $\sim 7 \times 10^{-110}$ s^{-1}. However, the assistance of QMT speeds up the reaction with a k_T of $\sim 9 \times 10^{-6}$ s^{-1}, which should lead to an experimentally observable

https://doi.org/10.1021/acs.jpcb.2c00218
J. Phys. Chem. B 2022, 126, 1799−1804

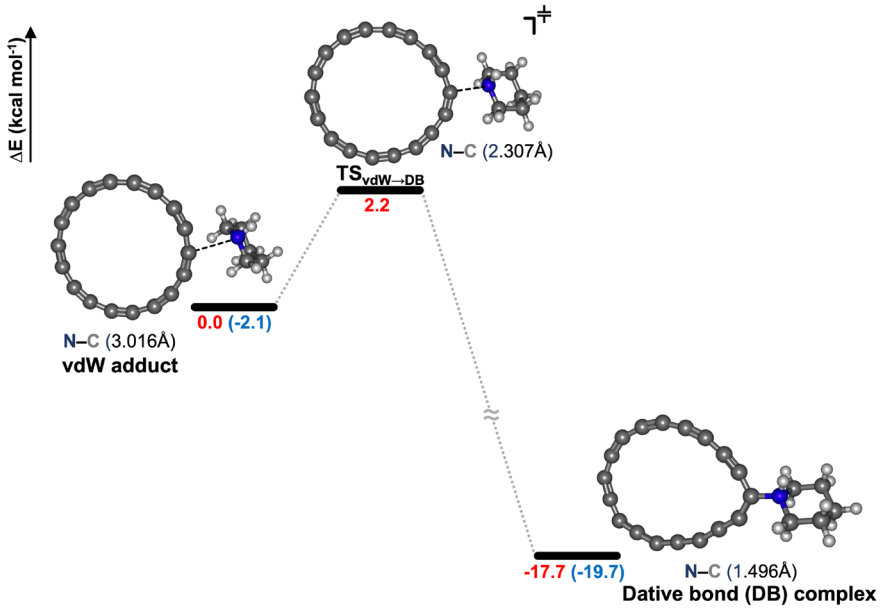

Figure 1. Double-well potential of C_{18}–pip complex in the piperidine solvent along with N–C bond distances. The relative energies are indicated in red, and the binding energies within parentheses are in blue.

rate. It can also be seen from Table 1 that as the temperature increases toward the 30 K sublimation temperature of the

Table 1. Semiclassical (k_{SC}) and Tunneling-Corrected (k_T) Rate Constants (in s^{-1}) and Half-Lives ($t_{1/2}$) (in s) for LB to SB Transformation in C_{18}–Pip Adducts from 4 to 30 K

T	k_{SC}	k_T	$t_{1/2}$
4	7×10^{-110}	9×10^{-6}	8×10^{4}
6	10^{-69}	9×10^{-6}	8×10^{4}
8	10^{-49}	10^{-5}	7×10^{4}
10	10^{-37}	2×10^{-5}	5×10^{4}
20	2×10^{-13}	4×10^{-4}	4×10^{4}
30	2×10^{-5}	0.02	38

argon matrix, the tunneling rate increases rapidly, yielding a k_T of 0.02 s^{-1}, corresponding to a half-life $t_{1/2}$ (calculated as $t_{1/2} = \ln 2/k$) of ∼38 s. This means that if we can observe the transformation of vdW → DB in an argon matrix doped with pip solvent, the vdW adduct will have a fleeting existence, and only the DB complex will be detected and isolated under matrix isolation spectroscopy. The transient behavior of the vdW complex can likewise be attributed to a similar case of quantum tunneling instability.[54] Noteworthy, our gas-phase reaction rates also reveal that QMT completely drives this reaction at low temperatures (see the Supporting Information for the rates table) as well as that at the liquid N_2 temperature (77 K) the vdW adduct ($t_{1/2}$ = 0.6 s) will have a fleeting existence. However, its k_T rates are slower compared to those in solvent, as expected due to the higher barrier and low exergonicity of the reaction (*vide supra*).

The Arrhenius plot depicted in Figure 2 clearly shows a divergence of the tunneling-corrected k_T rates (curved line) from the semiclassical k_{SC} rate constants (straight line) and reaching a plateau as the temperature is lowered, further strengthening the case for QMT in the studied system.

Up to about 50 K, the role of QMT still dominates the overall reaction rate, but in this regime, excited vibrational

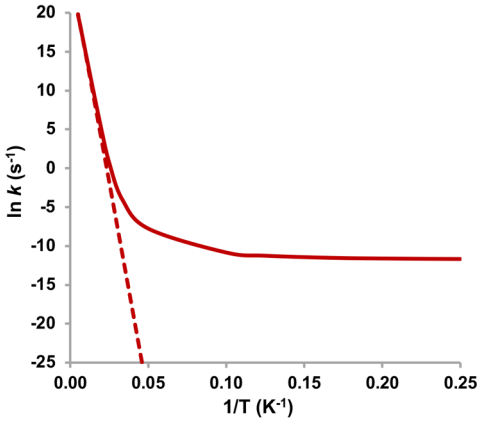

Figure 2. Arrhenius plot of the k_{SC} (dashed line) or k_T (solid line) against the inverse of temperature for a temperature range of 4–200 K.

levels of the molecules acquire significant population and QMT occurs from there by a thermally activated tunneling process.[55] Note that as opposed to hydrogen-tunneling-based reactions where the vibrational energy levels are well-separated, the energy levels in the case of heavy-atom tunneling are compact and closely spaced, making the molecules easily accessible to higher vibrational energy levels even with a small amount of heat; therefore, we see a softer concave Arrhenius graph in the thermally activated tunneling regime.

We further analyzed the kinetic isotope effect (KIE), a standard probe for the "fingerprint" of QMT in a chemical reaction. Our computed tunneling-corrected KIEs of the atoms involved along the reaction axis, i.e., nitrogen and carbon of the N–C bond (KIE calculated as $^{12}C/^{13}C$ for carbon and $^{14}N/^{15}N$ for nitrogen) gives a maximum KIE of 1.41 and 2.99 at 4 K, respectively, indicating a clear case of heavy-atom QMT; however, among them the exceptionally higher KIE value of nitrogen (possibly a record for this atom) suggests that it is the "tunneling-determining atom",[56] i.e., the atom with the

https://doi.org/10.1021/acs.jpcb.2c00218
J. Phys. Chem. B 2022, 126, 1799–1804

Table 2. N−C Bond Distance for van der Waals (vdW), Dative Bond (DB), and Transition State (TS) Structures in Å, Their Respective Binding Energies (BE) along with Threshold Energies (from LB to TS, $\Delta E^{\ddagger}$), Reaction Energies (ΔE_r) in kcal mol^{-1}, Transition State Imaginary Frequencies (υ) in cm^{-1}, and Semiclassical (k_{SC}) and Tunneling (k_T) Rates in s^{-1} at 4 K for the Studied C_n−Pip Complexes

system	vdW	DB	TS	BE_{vdW}	BE_{DB}	$\Delta E^{\ddagger}$	ΔE_r	υ	k_{SC}	k_T
C_{14}−pip	2.914	1.489	2.536	−1.8	−29.0	0.1	−27.2	115i	6×10^{5}	7×10^{9}
C_{16}−pip	2.934	1.501	2.380	−2.3	−23.5	1.2	−21.2	150i	4×10^{-56}	100
C_{18}−pip	3.016	1.496	2.307	−2.1	−19.7	2.2	−17.7	164i	7×10^{-110}	9×10^{-6}
C_{20}−pip	2.989	1.504	2.241	−2.1	−17.0	2.8	−14.9	164i	2×10^{-142}	2×10^{-7}
C_{22}−pip	3.016	1.505	2.207	−2.0	−14.6	3.5	−12.6	207i	5×10^{-182}	9×10^{-12}

most dominant influence on the tunneling rates. As the reaction involves significant deformation of the C_{18} ring during the formation of the DB complex, we also computed the KIE on the ring carbons by substituting all of the 18 carbons by their heavier isotope in order to preserve symmetry during the reaction progress. This yields a surprisingly large KIE of 2.58 at 4 K, reflecting that all the carbons participate in the tunneling process. Furthermore, we also computed the KIE of hydrogen (H/D) attached to the nitrogen, which exhibits a large displacement during the reaction progress, and obtained a value of 2.21 at 4 K, giving an indication of hydrogen tunneling. However, because of its small atomic mass and the large mass disparity with its isotopologues (H/D), the KIE cannot be compared to the ratio of heavier atom counterparts, but it is clear that within the heavy atoms the nitrogen of the pip has a more decisive influence on the overall QMT rate.

We have also explored the double-well potentials of the complexes formed by analogues of C_{18}, namely, C_{14} to C_{22} (see Table 2). All these systems considered here are closed-shell singlet ground states.[23,57,58] The N−C bond lengths and its binding energy (BE) strength of the vdW form of these complexes are almost invariant except for C_{14}−pip, which has the smallest BE. On the other hand, the bond distance of the DB complexes increases with increasing cyclo[n]carbon ring size, and their corresponding BEs decrease. The threshold barrier for the vdW → DB conversion is predicted to be lower with decreasing ring size and high exergonicity of the reaction showing Hammond's postulate type correlation.[24] This trend in the $\Delta E^{\ddagger}$ and ΔE_r is due to the fact that in going from C_{14} to C_{22}, what Hobza termed the "strain energy", i.e., the energy required for ring deformation during complexation, increases, thereby explaining the higher $\Delta E^{\ddagger}$ and destabilizing ΔE_r.[23] Notably, we have also studied smaller complexes formed by C_{10} and C_{12}; however, it exhibits a barrierless flat potential yielding a single minimum-energy configuration with an N−C bond distance of 1.496 and 1.487 Å and BE of −39.4 and −37.5 kcal mol^{-1} for the former and latter, respectively.

Turning next to the QMT rates for the donor−acceptor complexes of these smaller analogues, our computations predict that the reactions are forbidden classically at 4 K except for C_{14}, for which the reaction is almost barrierless, making the reaction feasible (see Table 2). However, the inclusion of tunneling correction in the overall rate constant accelerates the reaction by several orders of magnitude in all the studied cases. As shown in Table 2, the k_T is extremely fast for the complexes with smaller C_{14} and C_{16} ring sizes, corresponding to a short half-life of 0.1 ns and 0.01 s at 4 K for the former and latter, suggesting that the vdW long-bond adduct is fleetingly stable. For larger C_{20} and C_{22} systems, the QMT rate is lower than for their smaller analogues (Table 2) with extremely more prolonged $t_{1/2}$ ranging from months to millennia at 4 K, indicating that only the vdW adduct will be isolable in a standard experimental setup. However, it should be mentioned that as the temperature is raised to 50 K, the role of thermally activated tunneling enhances the overall reaction rate in all the above systems, making the vdW complex's existence fleeting (see the Supporting Information for the full rates table). For instance, the k_T for C_{20}−pip and C_{22}−pip results in a value of 0.7 and 5×10^{-4} s^{-1} at 50 K with $t_{1/2}$ of 0.9 s and ∼20 min. The slow QMT rates for the larger systems can be attributed to the higher threshold barrier and less exergonicity of the reaction, which can produce a wider barrier width.

Because an accurate estimation of the barrier width (w) is difficult to determine—as real reactions do not exhibit a simple square or inverse parabolic PES, but instead run through a roughly Gaussian-shaped minimum-energy path (MEP)[25,59]—we therefore considered the potential energy profiles of the MEP (V_{mep}) with respect to the mass-scaled reaction coordinate (s) (see Figure 3) and the changes of the ground state vibrational adiabatic potential energy curve [$V_a^G(s)$] along the reaction coordinate (s) (see Figure S1 in the Supporting Information) as a visual indicator of the influence of w on the tunneling rate differences in C_n−pip systems. It can be seen clearly from Figure 3 that with the increase in the size of the cyclocarbon ring w gets wider along with higher $\Delta E^{\ddagger}$, which nicely explains the reason for the decreasing QMT rates from C_{14}−pip to C_{22}−pip.

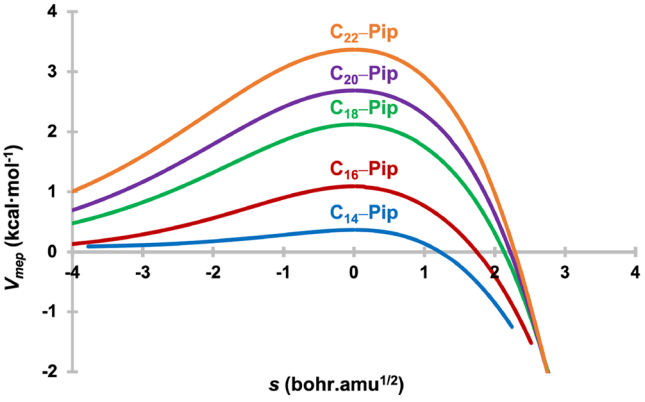

Figure 3. Minimum-energy-path potential (V_{mep}) as a function of the reaction coordinate (s) in mass-scaled coordinates for the studied C_n−pip complexes.

CONCLUSION

In summary, our rate constant calculations including multidimensional tunneling correction reveal the overwhelming role of heavy atom QMT in the vdW → DB transformation of the

https://doi.org/10.1021/acs.jpcb.2c00218
J. Phys. Chem. B 2022, 126, 1799−1804

C_{18}−pip complex at cryogenic temperatures where the classical over-the-barrier process is virtually nonexistent. At the sublimation temperature of the argon matrix (30 K), the decay QMT rate is predicted to be extremely fast with a $t_{1/2}$ of only 38 s, indicating the fleeting existence of vdW complex. The concave Arrhenius graph and the KIE analysis further sharpen the fingerprint of QMT in this reaction. Additionally, we explored the role of QMT in other C_n−pip systems (n = 14, 16, 20, and 22) and predicted a rapid QMT rate for the smaller analogues of C_{18}, with very to extremely short $t_{1/2}$ ranging between seconds and nanoseconds at 4 K. The present study shows that QMT can play a determining role in the covalent/dative bond formation of C_{18}−pip. Considering the recent work on the enhanced stability of C_{60} with pip, it remains to be tested if tunneling can act a key player in the covalent/dative bond functionalization of fullerenes.

■ ASSOCIATED CONTENT

Supporting Information

The Supporting Information is available free of charge at https://pubs.acs.org/doi/10.1021/acs.jpcb.2c00218.

Table of CVT and SCT rate constants as a function of temperature; polyrate input and output details; vibrational adiabatic potential energy profile; all relevant geometries in XMol/Molden.XYZ format; full references of Gaussian 16 and Polyrate17 (PDF)

■ AUTHOR INFORMATION

Corresponding Authors

Ashim Nandi − *Department of Molecular Chemistry and Materials Science, Weizmann Institute of Science, 7610001 Reḥovot, Israel;* orcid.org/0000-0002-1090-7664; Email: ashim.nandi@weizmann.ac.il

Jan M. L. Martin − *Department of Molecular Chemistry and Materials Science, Weizmann Institute of Science, 7610001 Reḥovot, Israel;* orcid.org/0000-0002-0005-5074; Email: gershom@weizmann.ac.il

Complete contact information is available at: https://pubs.acs.org/10.1021/acs.jpcb.2c00218

Notes

The authors declare no competing financial interest.

■ ACKNOWLEDGMENTS

This research was supported in part by the Israel Science Foundation (Grant 1969/20) and the Minerva Foundation (Grant 2020/05). A.N. acknowledges the Feinberg Graduate School of the Weizmann Institute for a Dean's Excellence Postdoctoral Fellowship.

■ REFERENCES

(1) Kaiser, K.; Scriven, L. M.; Schulz, F.; Gawel, P.; Gross, L.; Anderson, H. L. An Sp-Hybridized Molecular Carbon Allotrope, Cyclo[18]Carbon. *Science* **2019**, *365* (6459), 1299−1301.

(2) Kroto, H. W.; Heath, J. R.; O'Brien, S. C.; Curl, R. F.; Smalley, R. E. C_{60} : Buckminsterfullerene. *Nature* **1985**, *318* (6042), 162−163.

(3) Iijima, S. Helical Microtubules of Graphitic Carbon. *Nature* **1991**, *354* (6348), 56−58.

(4) Novoselov, K. S.; Geim, A. K.; Morozov, S. V.; Jiang, D.; Zhang, Y.; Dubonos, S. V.; Grigorieva, I. V.; Firsov, A. A. Electric Field Effect in Atomically Thin Carbon Films. *Science* **2004**, *306*, 666.

(5) Baryshnikov, G. V.; Valiev, R. R.; Kuklin, A. V.; Sundholm, D.; Ågren, H. Cyclo[18]Carbon: Insight into Electronic Structure, Aromaticity, and Surface Coupling. *J. Phys. Chem. Lett.* **2019**, *10*, 6701−6705.

(6) Nandi, A.; Solel, E.; Kozuch, S. Carbon Tunneling in the Automerization of Cyclo[18]Carbon. *Chem.—Eur. J.* **2020**, *26* (3), 625−628.

(7) Brémond, É.; Pérez-Jiménez, Á. J.; Adamo, C.; Sancho-García, J. C. sp-Hybridized Carbon Allotrope Molecular Structures: An Ongoing Challenge for Density-Functional Approximations. *J. Chem. Phys.* **2019**, *151* (21), 211104.

(8) Stasyuk, A. J.; Stasyuk, O. A.; Solà, M.; Voityuk, A. A. Cyclo[18]Carbon: The Smallest All-Carbon Electron Acceptor. *Chem. Commun.* **2020**, *56* (3), 352−355.

(9) Hussain, S.; Chen, H.; Zhang, Z.; Zheng, H. Vibrational Spectra and Chemical Imaging of Cyclo[18]Carbon by Tip Enhanced Raman Spectroscopy. *Chem. Commun.* **2020**, *56* (15), 2336−2339.

(10) Lu, T.; Chen, Q. Ultrastrong Regulation Effect of the Electric Field on the All-Carboatomic Ring Cyclo[18]Carbon. *ChemPhysChem* **2021**, *22* (4), 386−395.

(11) Qin, B.; Zhang, Q.; Li, Y.; Yang, G.; Yu, H.; Peng, F. Mechanistic Insights into the Electrochemical Reduction of CO_2 on Cyclo[18]Carbon Using Density Functional Theory Calculations. *ChemElectroChem.* **2020**, *7* (8), 1838−1842.

(12) Zhang, L.; Li, H.; Feng, Y. P.; Shen, L. Diverse Transport Behaviors in Cyclo[18]Carbon-Based Molecular Devices. *J. Phys. Chem. Lett.* **2020**, *11*, 2611.

(13) Jiang, Y.; Jun Mattioli, E.; Calvaresi, M.; Wang, Z. Theoretical Design of an Ultrafast Supramolecular Rotor Composed of Carbon Nano-Rings. *Chem. Commun.* **2020**, *56* (79), 11835−11838.

(14) Fang, S.; Hu, Y. H. Cyclo[18]Carbon as an Ultra-Elastic Molecular O-Ring with Unique Mechanical Properties. *Carbon* **2021**, *171*, 96−103.

(15) Liu, Z.; Lu, T.; Chen, Q. Intermolecular Interaction Characteristics of the All-Carboatomic Ring, Cyclo[18]Carbon: Focusing on Molecular Adsorption and Stacking. *Carbon* **2021**, *171*, 514−523.

(16) Dai, C.; Chen, D.; Zhu, J. Achieving Adaptive Aromaticity in Cyclo[10]Carbon by Screening Cyclo[n]Carbon (N = 8−24). *Chem.—Asian J.* **2020**, *15* (14), 2187−2191.

(17) Charistos, N. D.; Munoz-Castro, A. Induced Magnetic Field in Sp-Hybridized Carbon Rings: Analysis of Double Aromaticity and Antiaromaticity in Cyclo[2 N]Carbon Allotropes. *Phys. Chem. Chem. Phys.* **2020**, *22* (17), 9240−9249.

(18) Liu, Z.; Lu, T.; Chen, Q. An sp-Hybridized All-Carboatomic Ring, Cyclo[18]Carbon: Bonding Character, Electron Delocalization, and Aromaticity. *Carbon* **2020**, *165*, 468−475.

(19) Lamanec, M.; Lo, R.; Nachtigallová, D.; Bakandritsos, A.; Mohammadi, E.; Dračínský, M.; Zbořil, R.; Hobza, P.; Wang, W. The Existence of a N→C Dative Bond in the C_{60}−Piperidine Complex. *Angew. Chem., Int. Ed.* **2021**, *133* (4), 1970−1978.

(20) Beck, M. T.; Mándi, G. Solubility of C_{60}. *Fullerene Sci. Technol.* **1997**, *5* (2), 291−310.

(21) Talukdar, S.; Pradhan, P.; Banerji, A. Electron Donor-Acceptor Interactions of C_{60} with n-And π-Donors: A Rational Approach Towards Its Solubility. *Fullerene Sci. Technol.* **1997**, *5* (3), 547−557.

(22) Solís-Fernández, P.; Okada, S.; Sato, T.; Tsuji, M.; Ago, H. Gate-Tunable Dirac Point of Molecular Doped Graphene. *ACS Nano* **2016**, *10* (2), 2930−2939.

(23) Lo, R.; Manna, D.; Hobza, P. Cyclo[n]Carbons Form Strong N → C Dative/Covalent Bonds with Piperidine. *J. Phys. Chem. A* **2021**, *125* (14), 2923−2931.

(24) Anslyn, E. V.; Dougherty, D. A. *Modern Physical Organic Chemistry*; University Science: Sausalito, CA, 2005.

(25) Castro, C.; Karney, W. L. Heavy-Atom Tunneling in Organic Reactions. *Angew. Chem., Int. Ed.* **2020**, *59* (22), 8355−8366.

(26) Meisner, J.; Kästner, J. Atom Tunneling in Chemistry. *Angew. Chem., Int. Ed.* **2016**, *55* (18), 5400−5413.

(27) Nandi, A.; Kozuch, S.; Kästner, J. Comment on "Computational Evidence for Sulfur Atom Tunneling in the Ring Flipping Reaction of S_4N_4. *Chem. Phys. Lett.* **2020**, *754*, 137678.

(28) Borden, W. T. Reactions That Involve Tunneling by Carbon and the Role That Calculations Have Played in Their Study. *WIREs Comput. Mol. Sci.* **2016**, *6* (1), 20−46.
(29) Karmakar, S.; Datta, A. Heavy-Atom Tunneling in Organic Transformations. *J. Chem. Sci.* **2020**, *132* (1), 127.
(30) Bell, R. P. *The Tunneling Effect in Chemistry*; Chapman and Hall: London, 1980.
(31) Schreiner, P. R. Quantum Mechanical Tunneling Is Essential to Understanding Chemical Reactivity. *Trends Chem.* **2020**, *2* (11), 980−989.
(32) Greer, E. M.; Cosgriff, C. V.; Doubleday, C. Computational Evidence for Heavy-Atom Tunneling in the Bergman Cyclization of a 10-Membered-Ring Enediyne. *J. Am. Chem. Soc.* **2013**, *135* (28), 10194−10197.
(33) Schleif, T.; Mieres-Perez, J.; Henkel, S.; Ertelt, M.; Borden, W. T.; Sander, W. The Cope Rearrangement of 1,5-Dimethylsemibullvalene-2(4)-D1: Experimental Evidence for Heavy-Atom Tunneling. *Angew. Chem., Int. Ed.* **2017**, *56* (36), 10746−10749.
(34) Zhang, X.; Hrovat, D. A.; Borden, W. T. Calculations Predict That Carbon Tunneling Allows the Degenerate Cope Rearrangement of Semibullvalene to Occur Rapidly at Cryogenic Temperatures. *Org. Lett.* **2010**, *12* (12), 2798−2801.
(35) Kozuch, S. Heavy Atom Tunneling in the Automerization of Pentalene and Other Antiaromatic Systems. *RSC Adv.* **2014**, *4* (41), 21650−21656.
(36) Nandi, A.; Sucher, A.; Kozuch, S. Ping-Pong Tunneling Reactions: Can Fluoride Jump at Absolute Zero? *Chem.—Eur. J.* **2018**, *24* (61), 16348−16355.
(37) Sedgi, I.; Kozuch, S. Heavy Atom Tunnelling on XeF_6 Pseudorotation. *Phys. Chem. Chem. Phys.* **2020**, *22* (31), 17725−17730.
(38) Nandi, A.; Sucher, A.; Tyomkin, A.; Kozuch, S. Ping-Pong Tunneling Reactions, Part 2: Boron and Carbon Bell-Clapper Rearrangement. *Pure Appl. Chem.* **2020**, *92* (1), 39−47.
(39) Schreiner, P. R. Tunneling Control of Chemical Reactions: The Third Reactivity Paradigm. *J. Am. Chem. Soc.* **2017**, *139* (43), 15276−15283.
(40) Gerbig, D.; Schreiner, P. R. Tunneling in the Reactions of Carbenes and Oxacarbenes. *Contemporary Carbene Chemistry* **2013**, 193−215.
(41) Nunes, C. M.; Eckhardt, A. K.; Reva, I.; Fausto, R.; Schreiner, P. R. Competitive Nitrogen versus Carbon Tunneling. *J. Am. Chem. Soc.* **2019**, *141* (36), 14340−14348.
(42) Nandi, A.; Tarannam, N.; Rodrigues Silva, D.; Fonseca Guerra, C.; Hamlin, T. A.; Kozuch, S. Boron Tunneling in the "Weak" Bond-Stretch Isomerization of N−B Lewis Adducts. *ChemPhysChem* **2021**, *22* (18), 1857−1862.
(43) Zhao, Y.; Truhlar, D. G. The M06 Suite of Density Functionals for Main Group Thermochemistry, Thermochemical Kinetics, Noncovalent Interactions, Excited States, and Transition Elements: Two New Functionals and Systematic Testing of Four M06-Class Functionals and 12 Other Functionals. *Theor. Chem. Acc.* **2008**, *120* (1), 215−241.
(44) Frisch, M. J.; Trucks, G. W.; Schlegel, H. B.; Scuseria, G. E.; Robb, M. A.; Cheeseman, J. R.; Scalmani, G.; Barone, V.; Petersson, G. A.; Nakatsuji, H. et al. *Gaussian 16*, Rev. C.01; Gaussian, Inc.: Wallingford, CT, 2019.
(45) Martin, J. M. L.; Bauschlicher, C. W.; Ricca, A. On the Integration Accuracy in Molecular Density Functional Theory Calculations Using Gaussian Basis Sets. *Comput. Phys. Commun.* **2001**, *133* (2), 189−201.
(46) Truhlar, D. G.; Garrett, B. C. Variational Transition State Theory. *Annu. Rev. Phys. Chem.* **1984**, *35* (1), 159−189.
(47) Fernandez-Ramos, A.; Ellingson, B. A.; Garrett, B. C.; Truhlar, D. G. Variational Transition State Theory with Multidimensional Tunneling. In *Reviews in Computational Chemistry*; Wiley-Blackwell: 2007; pp 125−232.
(48) Skodje, R. T.; Truhlar, D. G.; Garrett, B. C. Vibrationally Adiabatic Models for Reactive Tunneling. *J. Chem. Phys.* **1982**, *77* (12), 5955−5976.
(49) Zheng, J.; Bao, J. L.; Meana-Pañeda, R.; Zhang, S.; Lynch, B. J.; Corchado, J. C.; Chuang, Y.-Y.; Fast, P. L.; Hu, W.-P.; Liu, Y.-P. et al. *Polyrate*, ver. 2017-C; University of Minnesota: Minneapolis, 2017.
(50) Zheng, J.; Zhang, S.; Corchado, J. C., Chuang, Y. Y.; Coitino, E. L.; Ellingson, B. A.; Truhlar, D. G. *GAUSSRATE*, ver. 2016; University of Minnesota: Minneapolis, MN, 2016.
(51) Page, M.; McIver, J. W. On Evaluating the Reaction Path Hamiltonian. *J. Chem. Phys.* **1988**, *88* (2), 922−935.
(52) Lauderdale, J. G.; Truhlar, D. G. Diffusion of Hydrogen, Deuterium, and Tritium on the (100) Plane of Copper: Reaction-Path Formulation, Variational Transition State Theory, and Tunneling Calculations. *Surf. Sci.* **1985**, *164* (2), 558−588.
(53) Tomasi, J.; Mennucci, B.; Cammi, R. Quantum Mechanical Continuum Solvation Models. *Chem. Rev.* **2005**, *105*, 2999−3093.
(54) Amlani, H.; Frenklah, A.; Kozuch, S. Chapter 2: Tunnelling Instability in Molecular Systems. An Exercise in Computational Chemistry Prediction Power. *Tunnelling in Molecules* **2020**, 61−87.
(55) Greer, E. M.; Kwon, K.; Greer, A.; Doubleday, C. Thermally Activated Tunneling in Organic Reactions. *Tetrahedron* **2016**, *72* (47), 7357−7373.
(56) Kozuch, S. The Reactivity Game: Theoretical Predictions for Heavy Atom Tunneling in Adamantyl and Related Carbenes. *Phys. Chem. Chem. Phys.* **2014**, *16* (17), 7718−7727.
(57) Lee, T. J.; Taylor, P. R. A Diagnostic for Determining the Quality of Single-Reference Electron Correlation Methods. *Int. J. Quantum Chem.* **1989**, *36* (S23), 199−207.
(58) Fogueri, U. R.; Kozuch, S.; Karton, A.; Martin, J. M. L. A Simple DFT-Based Diagnostic for Nondynamical Correlation. *Theor. Chem. Acc.* **2013**, *132* (1), 1291.
(59) Nandi, A.; Alassad, Z.; Milo, A.; Kozuch, S. Quantum Tunneling on Carbene Organocatalysis: Breslow Intermediate Formation via Water-Bridges. *ACS Catal.* **2021**, *11* (24), 14836−14841.

https://doi.org/10.1021/acs.jpcb.2c00218
J. Phys. Chem. B 2022, 126, 1799−1804